Chapter 2.
Analytic Models

2.1. Introduction

The basic picture that a nearly axisymmetric collision produces an outward propagating ring of high density and high star formation rate has been worked out by a number of investigators (Lynds & Toomre 1986; Toomre 1978; Appleton & Struck-Marcell 1987b; Struck-Marcell & Appleton 1987; Struck-Marcell & Lotan 1990; Theys & Spiegel 1977; Huang & Stewart 1988; Chatterjee 1984). If the collision is not axisymmetric, off-center rings, arcs and spiral patterns can be formed (Toomre & Toomre 1972; Toomre 1978; Struck-Marcell 1990; Chatterjee 1986, Huang & Stewart 1988; Gerber, Lamb & Balsara 1992). In order to understand the mechanism by which off-center collisions produce disturbed morphologies in galactic disks a simplified analytic model can provide insight. Further, an analytic model can be used economically to explore parameter space and guide the choice of future fully three-dimensional gravitational/hydrodynamical computational models of observed systems.

In this chapter it is shown that the disk morphologies produced by Toomre's n-body experiments on ring galaxies (Toomre 1978, see also Byrd & Howard 1992) can be understood in terms of an impulsive encounter with a second galaxy which produces epicyclic oscillations in the disk galaxy (see Section 2.2; Binney & Tremaine 1987; Struck-Marcell & Lotan 1990). Some of the results are similar to those obtained by Struck-Marcell (1990), but he was more interested in the development and classification of caustic structures in the disk following slightly off center collisions. The motivation for undertaking this study is to gain insight into the mechanism whereby high gas density regions are produced in numerical n-body/gas dynamics simulations (see Chapter 4). This work also differs from Struck-Marcell (1990) in that an arbitrarily large impact parameter is explicitly included, the restriction that the azimuthal velocity impulse be

small compared to the radial velocity impulse is lifted, and the central concentration of the intruder can be varied.

Analytic expressions are derived to describe the two-dimensional kinematic evolution of a stellar disk perturbed by the collision of a second galaxy which passes through the disk at perpendicular incidence, but does not pass through its center. The intruding galaxy is approximated as spherical and the disk stars of the host galaxy lie in a potential that produces a constant circular rotation velocity. The resulting morphologies depend on a "strength" parameter (see Section 2.2.2), the impact parameter, and the central concentration of the spherical galaxy.

The purely kinematic model can not yield information about the role of self gravity and gas dynamical processes, which are likely important for determining the sites of enhanced star formation. The behavior predicted by the analytic expressions is therefore compared with computational results from a fully self-gravitating three-dimensional n-body/gas dynamics code in Section 4.4. There is it shown that the initial behavior of the galaxies is similar to that predicted by the analytic model, but at later times in the evolution of the disk, self-gravity becomes important in amplifying density enhancements. Gas piles up where orbits cross since, unlike the stars, gas cannot freely move on intersecting orbits. It is argued that these regions of high gas density are likely to be the locations of active star formation.

The analytic model for the velocity impulse is described in Section 2.2. The kinematic response predicted by the model is presented in Section 2.3. A summary is given in Section 2.4.

2.2. Analytic Model

Under the simplifying assumptions described in the following sections, the equations of motion are derived for disk stars following a collision with a spherically symmetric galaxy. The intruder hits the disk at normal incidence at an arbitrary distance from the center. Using these equations of motion, which are shown to be functions of a star's

initial position and three dimensionless parameters, the kinematic morphology of the disk can be determined at any arbitrary time after the collision.

2.2.1. Solution for Velocity Impulses

The velocity impulse delivered by the intruder as it flies through the disk galaxy at constant velocity is first derived. The impulse approximation is expected to be valid as long as the intruder moves fast enough that the disk stars do not have time to move appreciably in their orbits during the interaction, but as mentioned in Binney & Tremaine (1987) this method can often be applied beyond its formal limits.

The geometrical configuration is illustrated in Fig. 2.2.1. The disk lies in the x-y plane, its center at the origin of coordinates. The intruder proceeds in a straight line in the x-z plane (the plane of the paper) parallel to the z axis at constant velocity V and penetrates the disk a distance x=b from the center of the disk. The vector $\vec{r}$ denotes position with respect to the center of the intruder while the vector $\vec{R}$, as well as the coordinates (x, y, z), refer to position with respect to the center of the disk.

The intruder is represented by a Plummer model (Plummer 1911); it provides an analytic model of a softened potential in which the degree of central concentration can be easily varied. The gravitational potential of the Plummer model is given by

$$\Phi = -\frac{GM}{(r^2 + a^2)^{1/2}}, \tag{2.2.1}$$

where G is the gravitational constant, M is the total mass of the Plummer model, and a is a constant, often referred to as a "softening" length since it introduces a length scale into the potential and prevents singular behavior at the origin. The velocity impulse delivered to a particle at a position $\vec{r}$ from the intruder is

$$\Delta\vec{v}\,(\vec{r}) = -\int_{-\infty}^{\infty} \nabla\Phi\,(\vec{r}, t)\; dt. \tag{2.2.2}$$

Substituting $\vec{r}(t) = (x - b)\hat{x} + y\hat{y} + (z + Vt)\hat{z}$, and taking the gradient of the potential yields,

$$(\nabla\Phi)_x = -\frac{GM\;(x - b)}{\left((x - b)^2 + (z + Vt)^2 + y^2 + a^2\right)^{3/2}} \tag{2.2.3a}$$

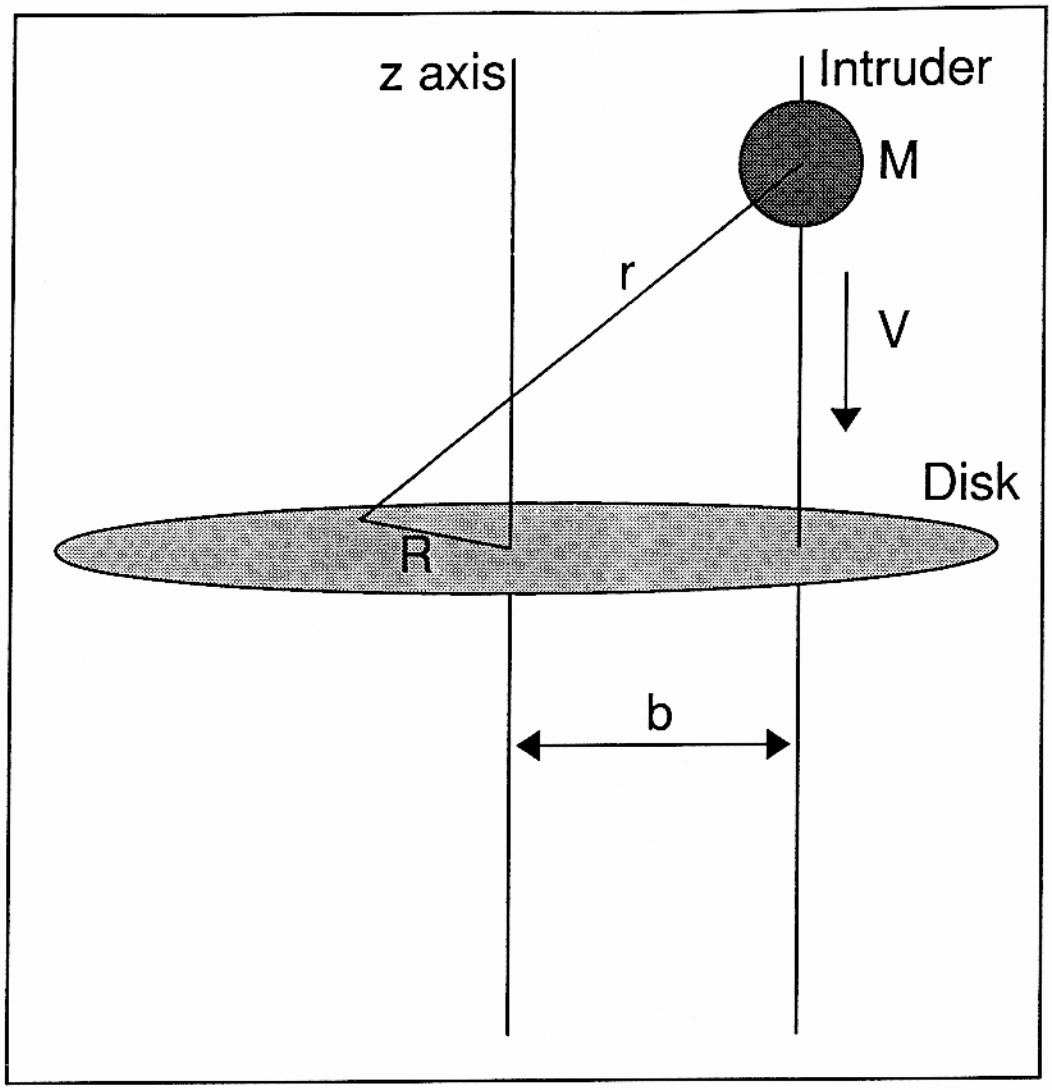

Figure 2.2.1: The geometrical configuration for the derivation of the impulse approximation expressions. The z-axis passes through the disk's center and the intruder moves along a line parallel to the z-axis, intersecting the plane of the disk a distance $x{=}b$ from its center. The intruder, of mass M, moves at constant velocity V.

$$(\nabla\Phi)_y = -\frac{GMy}{\left((x-b)^2+(z+Vt)^2+y^2+a^2\right)^{3/2}} \qquad (2.2.3b)$$

$$(\nabla\Phi)_z = -\frac{G\,M\,(z+Vt)}{\left((x-b)^2+(z+Vt)^2+y^2+a^2\right)^{3/2}} \tag{2.2.3c}$$

Upon performing the integrations of Equation (2.2.2), we obtain

$$\Delta\vec{v}\,(x,y,z) = -\frac{2\,G\,M}{V}\left[\frac{(x-b)\,\hat{x}+y\hat{y}}{(x-b)^2+y^2+a^2}\right]. \tag{2.2.4}$$

Rewriting this result in polar coordinates, (R,ϕ) defined by $x = R\cos\phi, y = R\sin\phi$, gives

$$\Delta\vec{v}\,(R,\phi) = -\frac{2\,G\,M}{V}\left[\frac{(R-b\cos\phi)\,\hat{R}+b\sin\phi\,\hat{\phi}}{R^2-2Rb\cos\phi+b^2+a^2}\right]. \tag{2.2.5}$$

The angular dependence is written in dimensionless form by defining the parameters, $\eta \equiv R/b$ and $\gamma \equiv a/b$ and we have

$$\Delta v_R = -\frac{2\,G\,M}{b\,V}\left[\frac{\eta-\cos\phi}{\eta^2-2\eta\cos\phi+1+\gamma^2}\right], \tag{2.2.6a}$$

$$\Delta v_\phi = -\frac{2\,G\,M}{b\,V}\left[\frac{\sin\phi}{\eta^2-2\eta\cos\phi+1+\gamma^2}\right]. \tag{2.2.6b}$$

2.2.2. Response to the Impulse

The effect the velocity impulse has on the orbits of stars in a given rigid potential will be investigated. First, equations 2.2.6 are modified to express the velocity relative to the impulse delivered to the center of the potential. Subtracting the velocity impulse delivered to the origin of coordinates from equations 2.2.6 we get

$$\Delta v_R = -\frac{2\,G\,M}{b\,V}\left[\frac{\eta-\cos\phi}{\eta^2-2\eta\cos\phi+1+\gamma^2}+\frac{\cos\phi}{1+\gamma^2}\right] \tag{2.2.7a}$$

$$\Delta v_\phi = -\frac{2\,G\,M}{b\,V}\left[\frac{\sin\phi}{\eta^2-2\eta\cos\phi+1+\gamma^2}-\frac{\sin\phi}{1+\gamma^2}\right]. \tag{2.2.7b}$$

The equations of motion for the disk particles are obtained by first assuming they were in circular orbits prior to receiving the impulse. After the interaction a particle orbit is described as executing epicyclic motion about a guiding center on a circular orbit of radius R_g. The value of R_g is obtained by determining the radius of the

circular orbit that has the same angular momentum as the particle *after* it received the impulse. The specific angular momentum, l_z, of a particle after the impulse is the sum of its initial angular momentum and the change in angular momentum delivered by the intruder,

$$l_z = R_0\, v_{c,0} + R_0\, \Delta v_\phi\,, \tag{2.2.8}$$

where R_0 is the initial radius and $v_{c,0}$ is the initial circular speed. The angular momentum associated with the guiding center's circular orbit is $R_g\, v_{c,g}$, where $v_{c,g}$ is the orbital speed of the guiding center. Equating the two expressions for the angular momentum and solving for R_g yields

$$R_g = R_0 \left(\frac{v_{c,0}}{v_{c,g}} + \frac{\Delta v_\phi}{v_{c,g}} \right) . \tag{2.2.9}$$

At this point the analysis is significantly simplified if it is assumed that the disk galaxy particles move in a potential which produces a rotation curve which is constant with radius. This is a reasonable simplification since most disk galaxies are observed to have constant rotation velocities over all but the inner portions of their disks. Under this assumption the previous equation becomes

$$R_g = R_0 \left(1 + \frac{\Delta v_\phi}{v_c} \right) \tag{2.2.10}$$

where v_c is the constant circular speed in the disk. The radial position of a particle is written as

$$R = R_g + A_R \sin(\kappa t + \Psi) \tag{2.2.11}$$

where κ is the epicycle frequency (determined by the potential) and A_R and Ψ are constants to be determined. For a particle which was initially at coordinates (R_0, ϕ_0) we demand that $R(t{=}0) = R_0$ and $\dot{R}(t{=}0) = \Delta v_R$, note that $\kappa = \sqrt{2} v_c / R$, and find, to lowest order in velocities,

$$\tan\Psi = -\sqrt{2} \frac{\Delta v_\phi}{\Delta v_R} . \tag{2.2.12}$$

Equivalently, we can write

$$\sin\Psi = -\sqrt{2} \frac{\Delta v_\phi}{\sqrt{2\Delta v_\phi^2 + \Delta v_R^2}} , \tag{2.2.13}$$

and

$$\cos\Psi = \frac{\Delta v_R}{\sqrt{2\Delta v_\phi^2 + \Delta v_R^2}}. \tag{2.2.14}$$

The amplitude to first order is

$$A_R = R_0 \frac{|\Delta\tilde{v}|}{\sqrt{2}v_c}. \tag{2.2.15}$$

where $|\Delta\tilde{v}| \equiv \sqrt{2\Delta v_\phi^2 + \Delta v_R^2}$. The expression for the radius then becomes

$$R = R_0 \left[1 + \frac{\Delta v_\phi}{v_c} + \frac{|\Delta\tilde{v}|}{\sqrt{2}v_c}\sin(\kappa t + \Psi)\right]. \tag{2.2.16}$$

The expression for the angular coordinate is found by demanding that angular momentum be conserved along the post-collision orbit. Equating the angular momentum after the collision with the angular momentum of the new guiding center yields

$$\dot{\phi}R^2 = v_c R_g\,. \tag{2.2.17}$$

Substituting the expression for R and keeping terms only to first order yields

$$\dot{\phi} = \frac{v_c}{R_g}\left[1 - \frac{2A_R}{R_0}\sin(\kappa t + \Psi)\right]. \tag{2.2.18}$$

This is integrated to give

$$\phi = \frac{v_c t}{R_0} + \frac{2A_R v_c}{\kappa R_0^2}\cos(\kappa t + \Psi) + constant\,. \tag{2.2.19}$$

The constant is obtained by setting $\phi(0) = \phi_0$, which yields

$$\phi = \phi_0 - \frac{\Delta v_R}{v_c} + \frac{v_c t}{R_0}\left(1 - \frac{\Delta v_\phi}{v_c}\right) + \frac{|\Delta\tilde{v}|}{v_c}\cos(\kappa t + \Psi)\,. \tag{2.2.20}$$

The following dimensionless parameters, which will prove useful later, are defined

$$\chi \equiv \frac{2GM}{bVv_c} \tag{2.2.21a}$$

$$\eta_{max} \equiv \frac{R_{max}}{b} \tag{2.2.21b}$$

$$\gamma' \equiv \frac{\gamma}{\eta_{max}} = \frac{a}{R_{max}} \tag{2.2.21c}$$

$$\tau \equiv \frac{v_c t}{2\pi R_{max}} \tag{2.2.21d}$$

where R_{max} is the maximum radial extent of the disk. Physically, χ is a parameter describing the "strength" of the interaction — $\chi/2\gamma$ is the maximum possible value of the velocity impulse in units of the (constant) circular speed in the disk. For the approximations to be formally valid $\chi/2\gamma$ must be less than one. η_{max} is the maximum extent of the disk in units of the impact parameter, and γ' is the ratio of the intruder softening length to the maximum disk radius. τ measures time in units of the rotation period of the outer edge of the disk.

Dimensionless velocity impulses are defined to be

$$\Delta u_R \equiv \frac{\Delta v_R}{v_c \chi} = -\left[\frac{\eta_0 - \cos\phi_0}{\eta_0^2 - 2\eta_0\cos\phi_0 + 1 + \gamma'^2\eta_{max}^2} + \frac{\cos\phi_0}{1+\gamma'^2\eta_{max}^2}\right], \qquad (2.2.22a)$$

$$\Delta u_\phi \equiv \frac{\Delta v_\phi}{v_c \chi} = -\left[\frac{\sin\phi_0}{\eta_0^2 - 2\eta_0\cos\phi_0 + 1 + \gamma'^2\eta_{max}^2} - \frac{\sin\phi_0}{1+\gamma'^2\eta_{max}^2}\right], \qquad (2.2.22b)$$

$$|\Delta\tilde{u}| \equiv \frac{|\Delta\tilde{v}|}{v_c\chi} = \sqrt{2\Delta u_\phi^2 + \Delta u_R^2}, \qquad (2.2.22c)$$

and the equations of motion are written, in terms of the ratio of radius to impact parameter, η, and angular position, ϕ, as

$$\eta = \eta_0\left\{1 + \chi\Delta u_\phi + \frac{\chi|\Delta\tilde{u}|}{\sqrt{2}}\sin\left(2\pi\sqrt{2}\frac{\eta_{max}}{\eta_0}\left(1-\chi\Delta u_\phi\right)\tau + \Psi\right)\right\} \qquad (2.2.23a)$$

$$\phi = \phi_0 - \chi\Delta u_R + 2\pi\frac{\eta_{max}}{\eta_0}\left(1-\chi\Delta u_\phi\right)\tau + \chi|\Delta\tilde{u}|\cos\left(2\pi\sqrt{2}\frac{\eta_{max}}{\eta_0}\left(1-\chi\Delta u_\phi\right)\tau + \Psi\right). \qquad (2.2.23b)$$

Note that these equations of motion depend only on the initial coordinates, (η_0, ϕ_0), and the three parameters χ, η_{max}, and γ'.

2.2.3. Surface Density

With the particle positions as functions of time and their original coordinates, we can demand that the mass, dM, in a small area be conserved and get an expression for the surface density, Σ.

$$dM = \Sigma(R,\phi,t)\; R\,dR\,d\phi = \Sigma(R_0,\phi_0)\; R_0\,dR_0\,d\phi_0\,. \qquad (2.2.24)$$

The coordinates are related through the determinant of the Jacobian matrix, J, by

$$dR\,d\phi = |J|\,dR_0\,d\phi_0\,, \tag{2.2.25}$$

and the surface density is

$$\Sigma(R,\phi) = \Sigma(R_0,\phi_0)\,\frac{R_0}{R}\,|J|^{-1}\,. \tag{2.2.26}$$

Formally the surface density goes to infinity at the zeros of the Jacobian. These points correspond to the caustics described by Struck-Marcell (1990) and Struck-Marcell & Lotan (1990) — regions where orbits overlap. In real galaxies these infinities are suppressed since (1) the density distribution is made up of discrete stars, more than one of which cannot occupy the same location, and (2) the stars are initially spread in phase space by virtue of a non-zero velocity dispersion. Hydrodynamic pressure forces (operating in three dimensions) help prevent infinite densities in the gaseous component of galaxies. Nevertheless, high densities are reached when gas interacts in these regions will be shown in Section 4.4.1.2.

2.3. Kinematic Response of the Disk

After the collision, the transient disk morphology at any given time is a function of the three parameters which represent the impact parameter, the "strength" and the central concentration of the intruder. The best way to get a feel for how the three parameters affect the collision is to plot a sample of disk "stars" for different values of the parameters.

2.3.1. A Survey of Forms

The form of the equations of motion in Equations 2.2.23 allows investigation of distant collisions by setting $\eta_{max} \leq 1$. More central collisions can be modeled by considering larger values of η_{max}. The other two parameters which govern the kinematic response of the disk are χ, the ratio of the magnitude of the velocity impulse to v_c

(the circular speed in the disk), and the ratio $\gamma' = a/R_{max}$ describing the central concentration of the Plummer model.

In Fig. 2.3.1 the response of stars to the velocity impulse is plotted at one-half a rotation period of the outer edge of the disk. The disk's rotation is counterclockwise. Initial positions for 10^4 "stars" are randomly chosen and plotted according to the model at $\tau = 0.5$. (Radii η were chosen randomly in the interval $[0 : \eta_{max}]$, which produces a surface density that falls off as $1/\eta$, and is useful for illustrating particle kinematics.) In each column of Fig. 2.3.1 the strength of the interaction, χ, and the softening parameter, γ', are held constant as the impact parameter is varied, taking values of $2.0, 1.0, 0.5$, and 0.25 in units of the disk maximum radius (ie., $\eta_{max} = .5, 1, 2, 4$). The impact distance from the center of the disk is indicated by the arrow at the bottom of each panel. The impact point can be located by mentally translating the arrow upward until one end lies on the disk center. The scale is the same for all plots in Fig. 2.3.1. The central concentration, γ', has the value 0.4 in Fig. 2.3.1 (a), 0.2 in Fig. 2.3.1 (b), and 0.8 in Fig. 2.3.1 (c). Representative values of $\chi = 0.25, 0.50$, and 0.75 were chosen for display. The most extreme combination of parameters strictly invalidates the assumptions in small regions of the disk, but does not generally affect the overall morphology of the system.

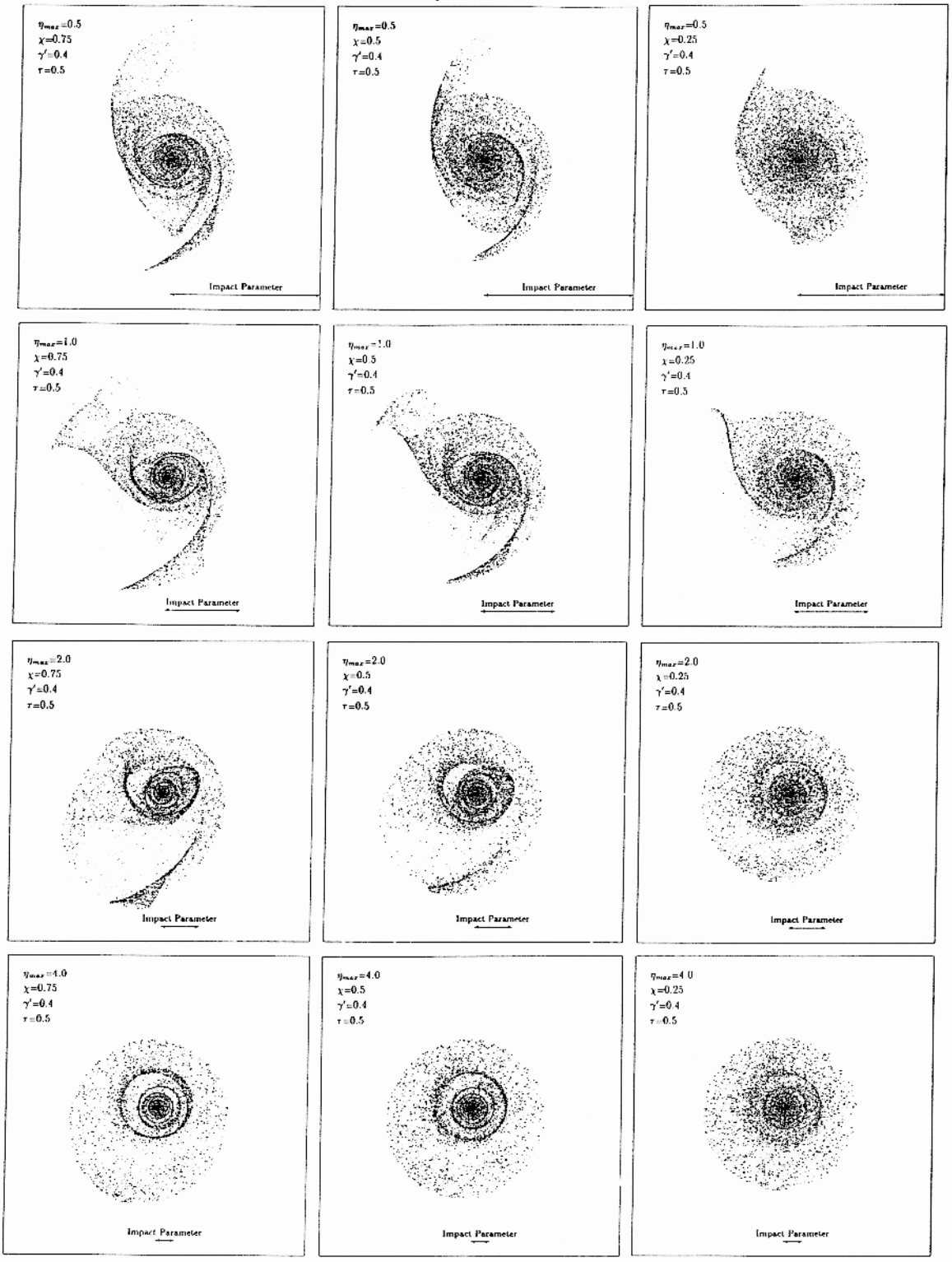

Figure 2.3.1: (a) Plots of disk particle positions as predicted by the analytic model. The impact parameter, indicated by the arrow, varies down each column. The "strength" decreases along each row. The parameter $\gamma' = 0.4$. See the text for a further explanation.

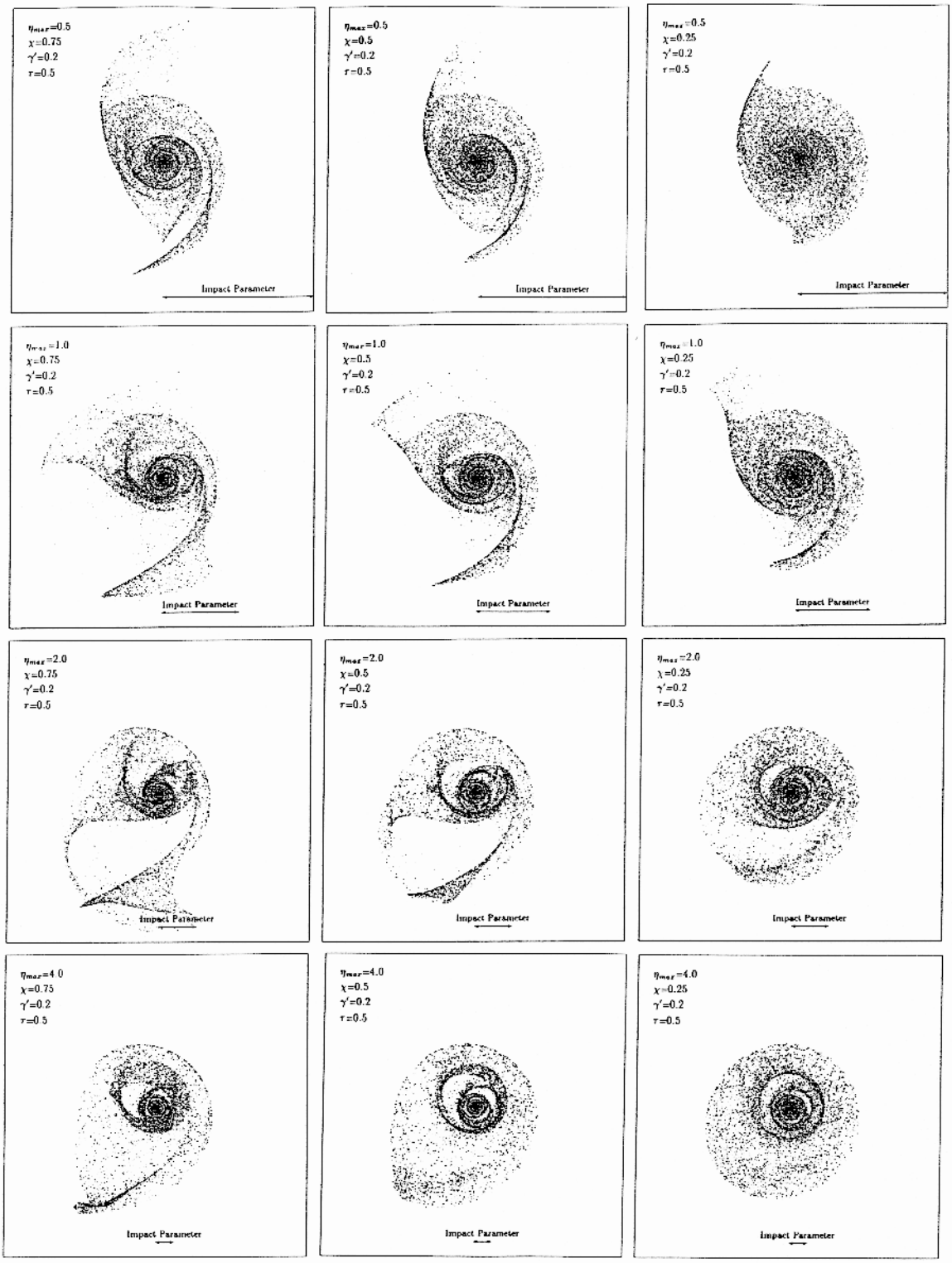

Figure 2.3.1: (b) The same as Fig. 2.3.1 (a), but with $\gamma' = 0.2$.

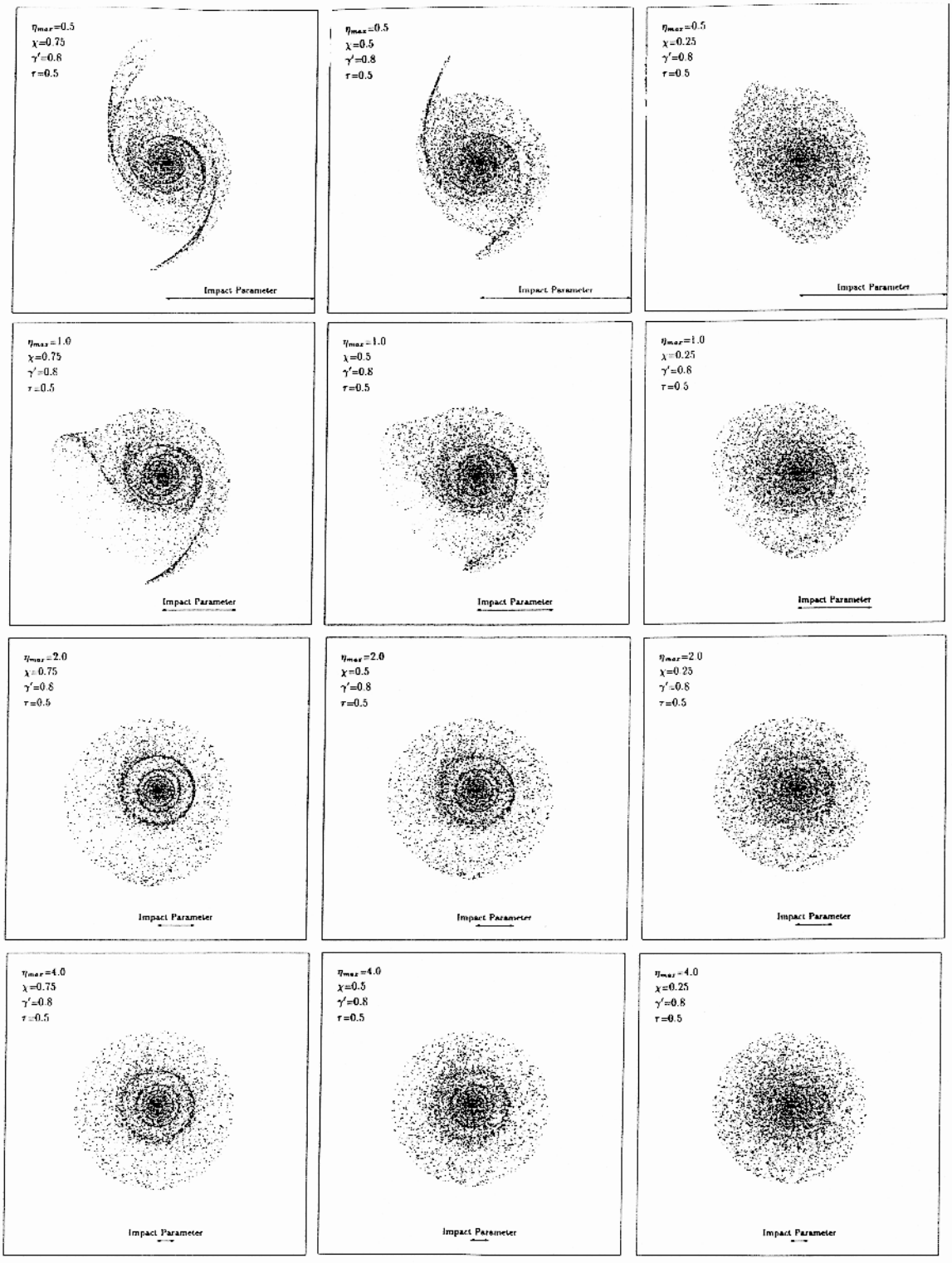

Figure 2.3.1: (c) The same as Fig. 2.3.1 (a), but with $\gamma' = 0.8$.

The dependence of morphology on the three parameters is shown in Fig. 2.3.1. More damage is done to the disks as the strength, χ, and the central concentration of the intruder (smaller γ') increase. The non-penetrating collisions (the first two rows in Fig. 2.3.1, ie. $\eta_{max} = 1, 0.5$) produce two-armed spiral features as exhibited in the n-body experiments of Toomre (1978). In the cases where the impact point is one-quarter the disk radius (row 4), rings form, although in the strongest interaction at this impact parameter $\eta_{max} = 4, \chi = 0.75, \gamma' = 0.2$ in Fig. 2.3.1 (b)) an arm also extends outward through the disk. At intermediate impact parameters a one-armed spiral pattern is more prevalent. With decreasing impact parameter a transition is seen that goes from two-armed spiral, through one-armed spirals, to formation of a ring. The transition from spiral to ring patterns appears to take place at impact parameters somewhere near 0.25 of a disk radius depending on the strength and concentration of the intruder, approximately in agreement with the results of the n-body experiments of Lynds & Toomre (1976) and especially Toomre (1978). This agreement exists even though Lynds & Toomre considered parabolic collisions with a 2:1 mass ratio between the galaxies, a situation in which one might not expect the impulse approximation to be applicable.

This transition can be understood qualitatively by considering the magnitude and directions of the imposed velocity impulses. In all cases there is a velocity component that produces a compression toward the line connecting the disk center and the intruder. When the center of the intruder does not penetrate the disk, there is only simple tidal stretching along this same line. Differential rotation shears this elongated form into a two-armed spiral pattern. When the intruder center penetrates the disk, however, on one side there is a compression, rather than a stretching, toward the impact point. The arm on that side of the disk disappears, being replaced by an arc that can appear as an inner ring, leaving the galaxy with one arm. As the impact point moves more toward the center, axisymmetry is approached and arms are replaced by rings.

As the strength parameter decreases the galaxies become less distorted and the morphologies tend toward more symmetric forms. Likewise, as the intruder becomes

more extended at the same strength, nearly symmetric rings appear more often. Note that the strong collision half way out in the disk with an extended intruder ($\chi = 0.75, \gamma' = 0.8$ in Fig. 2.3.1 (c)) forms a ring.

The morphologies produced in the grazing encounters (η_{max}=1, .5) correspond closely to those found numerically by Byrd & Howard (1992) in a collision inclined by 40° to the disk normal. Their Figure 3 exhibits the same near and far side arm structure as seen the model discussed here. Byrd & Howard suggest that encounters at approximately 60° from the disk are most common and are important for the formation of grand design spirals. The ring and arm morphology evident in Barnes' (1992) n-body study (see his Figure 3) also mimics forms produced by the model.

2.3.2. Lifetimes of Features

Kinematic features typically appear to remain in the disk for tens of rotation periods of the outer disk before phase mixing washes out all obvious patterns (see Section 4.4.1.1). With galactic disk rotation periods on the order of a few 10^8 years, then kinematic features persist for 10^9 to 10^{10} years. It might be expected that dynamical processes would completely dominate the disk in a much shorter time, and Sundelius et al. (1987) have shown numerically that tidal arms can last some 3×10^9 years for a typical galaxy. Byrd & Howard (1992) conclude that these perturbations are important in driving spiral structure. Presumably processes such as swing amplification (Toomre 1981) are contributing to the longevity of the spiral structure in the dynamical simulations. But even in the absence of dynamics, a single passage of a low-mass intruder can initiate a very long-lived dramatic morphological response.

2.4. Summary

A kinematic model was derived for the collision of disk galaxy with a small, fast spherical galaxy which moves parallel to the disk galaxy's rotation axis, but does not pass through the center of the disk. This model shows that the the morphological forms found in the n-body experiments of Toomre (1978) and Byrd & Howard (1992) can be understood in terms of stars executing epicyclic oscillations about a circular guiding center in the plane of the disk after receiving a velocity impulse from a second galaxy. Use of these analytic expressions provide a convenient and computationally inexpensive method to search parameter space in preparation for full n-body/gas dynamics models of observed systems. The resulting morphologies depend on the "strength" parameter (which includes the mass and relative velocity of the intruder), the impact parameter, and the central concentration of the intruder. Distant encounters produce transient two-armed spiral features, collisions through the outer parts of the disk make one-armed spirals, and central collisions produce rings.